

# Phase-space structure of two-dimensional excitable localized structures

Damià Gomila,<sup>\*</sup> Adrian Jacobo,<sup>†</sup> Manuel A. Matías,<sup>‡</sup> and Pere Colet<sup>§</sup>

*Instituto Mediterráneo de Estudios Avanzados, IMEDEA (CSIC-UIB), E-07122 Palma de Mallorca, Spain<sup>¶</sup>*

(Dated: Published: February 28, 2007)

In this work we characterize in detail the bifurcation leading to an excitable regime mediated by localized structures in a dissipative nonlinear Kerr cavity with a homogeneous pump. Here we show how the route can be understood through a planar dynamical system in which a limit cycle becomes the homoclinic orbit of a saddle point (saddle-loop bifurcation). The whole picture is unveiled, and the mechanism by which this reduction occurs from the full infinite-dimensional dynamical system is studied. Finally, it is shown that the bifurcation leads to an excitability regime, under the application of suitable perturbations. Excitability is an emergent property for this system, as it emerges from the spatial dependence since the system does not exhibit any excitable behavior locally.

PACS numbers: 05.45.-a, 42.65.Sf, 89.75.Fb

## I. INTRODUCTION

Localized structures (LS), or dissipative solitons, are spatio-temporal structures that appear in certain dissipative media [1], and, in particular, they have been found in a variety of systems, such as chemical reactions [2, 3], gas discharges [4] or fluids [1], among others. They are also found in optical cavities, due to the interplay of different effects, like diffraction, nonlinearity, driving, and dissipation [5, 6]. These structures, also known in this field as cavity solitons, have to be distinguished from conservative solitons found, for example, in propagation in fibers, for which there is a continuous family of solutions depending, e.g., on the initial conditions. Instead, dissipative solitons are unique once the parameters of the system have been fixed. This fact makes these structures potentially useful in optical (i.e., fast and spatially dense) storage and processing of information [6, 7, 8].

Here we consider the dynamics of LS in Kerr cavities, known as Kerr cavity solitons, that arise as a consequence of a modulational (namely a pattern-forming) instability of a homogeneous solution. In particular, they exist in the parameter range where the homogeneous solution coexists with stable subcritical (hexagonal) patterns. They share some properties with propagating spatial (conservative) solitons in a Kerr medium, but there are interesting differences. While in one transverse dimension (1D) Kerr spatial solitons are stable, it is well known that their 2D counterparts are unstable against self-focusing collapse [9]. The stability and dynamics of 2-D Kerr cavity solitons are thus of particular interest, and their existence and stability has been studied in several papers [10, 11, 12].

Localized structures may develop instabilities like start

moving, breathing or oscillating. In the latter case, LS oscillate in time while remaining stationary in space, like the oscillons found in a vibrated layer of sand [13]. Oscillating LS are autonomous oscillons, and have been reported both in optical [11, 12, 14] and chemical systems [15], and appear when the LS exhibits a Hopf bifurcation. In the present work we report on a route in which autonomous oscillating LS are destroyed, leading to an excitability regime, extending upon the results advanced in letter form in Ref. [16].

Typically a system is said to be excitable if while it sits at a stable fixed point, perturbations beyond a certain threshold induce a large response before coming back to the rest state. In phase space [17, 18] excitability occurs for parameter regions where a stable fixed point is close to a bifurcation in which an oscillation is created. Basically, there are two types of excitability: one characterized by a response time (to come back to the fixed point) within a relatively narrow range, also called Class II, and occurring in the well known FitzHugh-Nagumo model, and also the case in which excitability is mediated by a saddle point, also called Class I, and that exhibits an unbounded distribution of response times. The route to excitability reported here corresponds to the latter type of excitability. An interesting feature of this system is that, while, typically, in excitable media excitability is also found locally, i.e., in the zero-dimensional system, here we report a system in which excitability is an emergent property: it is not present at the local level but it appears through a property of an spatio-temporal structure exhibited by the system.

In the route reported in this work oscillating LS are made unstable in a global bifurcation, namely a saddle-loop bifurcation, in which a limit cycle becomes the homoclinic orbit of a saddle point. This bifurcation may occur generically in 2-variable continuous dynamical systems. Instead, the extended system studied here lives in an infinite-dimensional phase space, and, moreover, does not exhibit a spectrum with two slow modes that clearly dominate the dynamics, so an study is performed to show how the relevant dynamical behavior can be reduced to a two-mode representation. This reduction is a common

<sup>\*</sup>Electronic address: damia@imedea.uib.es

<sup>†</sup>Electronic address: jacoboa@imedea.uib.es

<sup>‡</sup>Electronic address: manuel@imedea.uib.es

<sup>§</sup>Electronic address: pere@imedea.uib.es

<sup>¶</sup>URL: <http://www.imedea.uib.es/physdept>

and powerful procedure to study the dynamics of spatial systems exhibiting coherent structures, however, the identification of the relevant modes is often highly non trivial.

The plan of this paper is as follows. First of all, the model and overall dynamical behavior exhibited by the system in parameter space are introduced in Sections II and III. Next, Section IV presents the case for the instability exhibited by LS through a saddle-loop bifurcation, discussing the main evidences to support this conclusion. Section V goes a step further in this direction, presenting a more detailed study of how the dynamics of the system can be understood through a simplified analysis, by performing an analysis in terms of modes. Finally, some concluding remarks are given in Section VIII.

## II. MODEL

A prototype model describing an optical cavity filled up with a nonlinear Kerr medium is the one introduced by Lugiato and Lefever [19] with the goal of studying pattern formation in this system. Later studies showed that this model also exhibits LS in some parameter regions [10, 11]. The model, obtained through the mean-field approximation, describes the dynamics of the slowly varying amplitude of the electromagnetic field  $E(\vec{x}, t)$  in the paraxial limit, where  $\vec{x} = (x, y)$  is the plane transverse to the propagation direction  $z$  on which the slow dynamics takes place. The time evolution of the electric field can be, then, written as

$$\frac{\partial E}{\partial t} = -(1 + i\theta)E + i\nabla^2 E + E_0 + i|E|^2 E \quad (1)$$

after suitably rescaling the variables.

The first term in the rhs describes cavity losses (making the system dissipative),  $E_0$  is the homogeneous (plane wave) input field,  $\theta$  the cavity detuning with respect to  $E_0$ , and  $\nabla^2 = \partial^2/\partial x^2 + \partial^2/\partial y^2$  is the transverse Laplacian modeling the diffraction. The sign of the cubic term indicates the so called self-focusing case. Notice that in the absence of losses and an input field, the field can be rescaled to  $E \rightarrow Ee^{i\theta t}$  to remove the detuning term and Eq. (1) becomes the Nonlinear Schrödinger Equation (NLSE). It is well documented that in the NLSE in two spatial dimensions an initial condition with enough energy collapses, namely energy accumulates at a point of space leading to the divergence of the solution at a finite time [20]. Cavity losses prevent this collapse, although in the parameter region in which localized structures are stable their dynamics are closely related to the collapse regime. Eq. (1) has a homogeneous steady state solution  $E_s = E_0/(1 + i(\theta - I_s))$ , where  $I_s = |E_s|^2$  [19]. In the following we use  $I_s$ , together with  $\theta$ , as our control parameters.

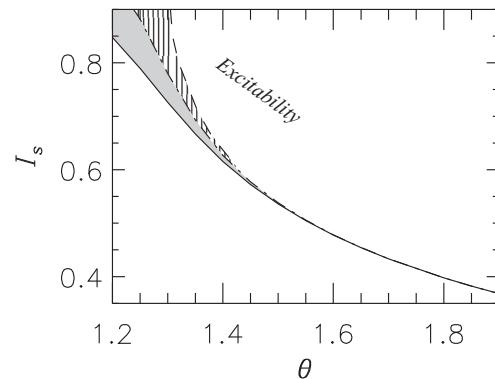


FIG. 1: Phase diagram of localized structures in the Kerr cavity. LS are stable in the shaded region and oscillate in the cross-hatched one (the dot-dashed line between these two regions indicates a Hopf bifurcation). In the lower part, below the saddle-node bifurcation (solid line), there are no LS, while in the upper part, above the saddle-loop bifurcation (dashed line), the system exhibits excitability.

## III. OVERVIEW OF THE SYSTEM BEHAVIOR

Performing a two-parameter study of the system, it has been shown that a stable regime of LS is found [12]. This region of existence in the parameter space is shown in Fig. 1. This regime occurs for  $I_s < 1$ , as at  $I_s = 1$  the so-called modulation instability takes place and the homogeneous solution becomes unstable, leading to the formation of hexagonal patterns [19, 21]. For  $I_s > 1$  the homogeneous solution continues to exist, although it is unstable. The hexagonal patterns are subcritical, namely through a S-shape branch and, thus, they coexist with the stable homogeneous solution for a certain parameter range.

This bistability regime is at the origin of the existence of stable LS, that appear when suitable (localized) transient perturbations are applied. The LS can be seen as a solution which connects a cell of the pattern with the homogeneous solution. While the existence of LS in this bistable regime is quite generic in extended systems, the stability of such LS strongly depends on the particular system. The mechanism by which LS appear is a saddle-node (or fold) bifurcation, as can be seen in Fig. 2 for  $\theta = 1.34$  and  $I_s \sim 0.655$  ( $|E_0|^2 \sim 4.5$ ) in which a pair of stable-unstable LS are created [22, 23].

The LS are rotationally symmetric around their center. Fig. 3 shows a transverse cut of typical upper and middle branch LS. The upper branch LS remains stable for a range of values of  $I_s$  and undergoes a Hopf bifurcation leading to a limit cycle when  $I_s$  is increased [10, 12, 24]. The region in parameter space where LS oscillate is shown in Fig. 1. Thus, in these conditions a LS is an autonomous oscillon. An interesting connection to the conservative case is that the growth of the LS during the oscillations resembles the collapse regime observed for the 2D (or 2 + 1) NLSE. In this case, however, after

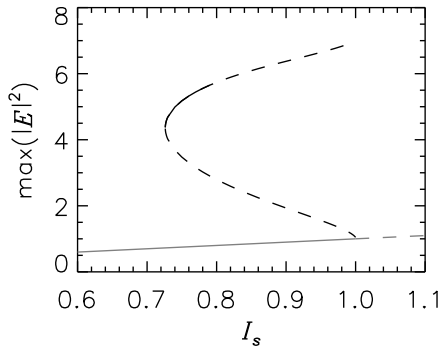


FIG. 2: Bifurcation diagram of stationary localized structures in the Kerr cavity:  $\max(|E|^2)$  vs  $I_s$  for  $\theta = 1.34$ . Solid lines represent stable solutions and dashed lines unstable ones. The lowest branch corresponds to the homogeneous solution that becomes unstable at  $I_s = 1.0$ . The upper and middle branches correspond to the stable and unstable LS, respectively, and are originated at a saddle-node bifurcation. The upper branch becomes Hopf unstable for larger values of  $I_s$ .

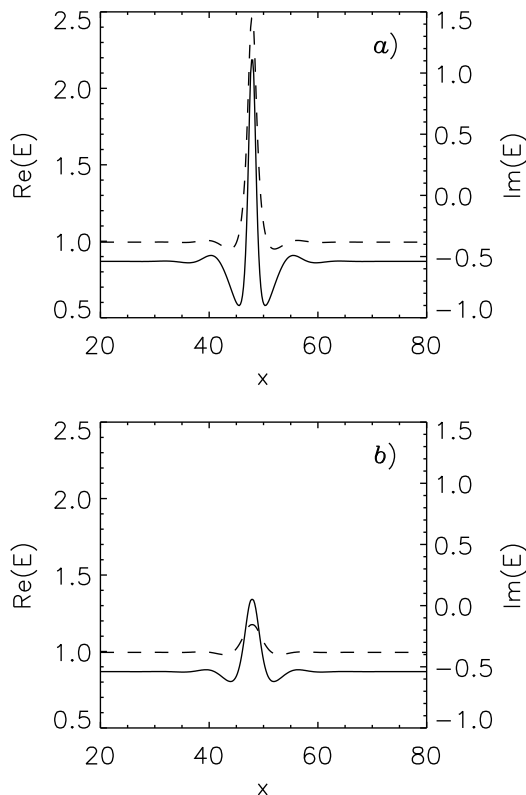


FIG. 3: Transverse cut of two LS, one from the upper (stable) branch a) and one from the middle (unstable) branch b) in Fig. 2 ( $I_s = 0.9$ ). The solid (dashed) line corresponds to  $\text{Re}[E]$  ( $\text{Im}[E]$ ).

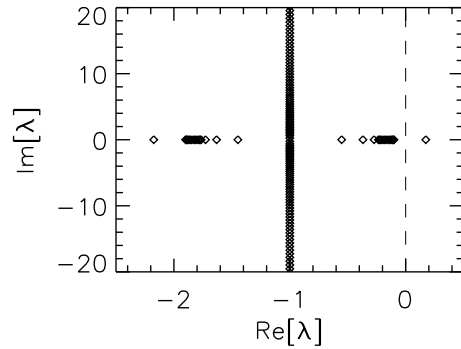


FIG. 4: Spectrum of the unstable (middle branch) LS for  $\theta = 1.30478592$  and  $I_s = 0.9$ .

some value is attained for the electric field,  $E$ , dissipation arrests this growth.

As  $I_s$  is further increased the amplitude of the limit cycle grows so that it gets closer to the unstable (middle) branch structure. It is perhaps surprising that the overall scenario can be understood qualitatively by resorting to a planar dynamical system, i.e., one with a two-dimensional phase space. These two phase space variables correspond to the amplitude of localized modes of the system (this issue is studied in detail in Section V). In the rest of the paper we will represent the main features of the behavior exhibited by the system in terms of these two-dimensional representation.

As shown in the Appendix, using a numerical method with arbitrary precision it is possible to determine the stability of the LS solutions. The spectrum of eigenvalues (of matrix  $\mathbf{U}$ , Eq. (7)) for an unstable (middle) branch LS is shown in Fig. 4. There is only one positive eigenvalue so this structure has a single unstable direction in the full phase space. In the reduced, planar phase space, it is a saddle point. Once it is created, the middle branch LS does not undergo any bifurcation for the parameter values explored in this paper and, so, remains a saddle point in phase space. When the limit cycle (corresponding to the oscillating LS) touches the middle branch the LS undergoes a so called *saddle-loop* bifurcation, that is the subject of Section IV. Beyond this bifurcation an excitable regime emerges, this regime will be described later in Section VI.

#### IV. SADDLE-LOOP BIFURCATION

A saddle-loop (also known as homoclinic or saddle-homoclinic) bifurcation is a global bifurcation in which a limit cycle becomes biasymptotic to a (real) saddle point, or, in other terms, becomes the homoclinic orbit of a saddle point (cf. [25, 26]), i.e., at criticality a trajectory leaving the saddle point through the unstable manifold returns to it through the stable manifold. Thus, at one

side of this bifurcation one finds a detached limit cycle (stable or unstable), while at the other side the cycle does not exist any more, only its *ghost*, as the bifurcation creates an exit slit that makes the system dynamics to leave the region in phase space previously occupied by the cycle. Thus, after the bifurcation the system dynamics jumps to another available attractor. In the present case this alternative attractor is the homogeneous solution.

Let us take  $\theta$  as the control parameter and assume that the saddle-loop bifurcation occurs for  $\theta = \theta_{SL}$ , and, for convenience, and without lack of generality, let us assume that  $\theta < \theta_{SL}$  corresponds to the oscillatory side, where the limit cycle is detached of the saddle point, while, in turn,  $\theta > \theta_{SL}$  corresponds to the side where one only has a fixed point solution. The fact that the bifurcation is global, implies that it cannot be detected locally (a local eigenvalue passing through zero), but one can still resort to the Poincaré map technique [34] to analyze it, and, interestingly, the main features of the bifurcation can be understood from the knowledge of the linear eigenvalues of the saddle.

The case studied here is the simplest: a saddle point with real eigenvalues, say  $\lambda_s < 0$  and  $\lambda_u > 0$ , in a 2-dimensional phase space. Strictly speaking, in our case the saddle has an infinite number of eigenvalues (Fig. 4), but only two eigenmodes take part in the dynamics close to the saddle. This will be studied in more detail in Sec. V. It is convenient to define the so called *saddle index*  $\nu = -\lambda_s/\lambda_u$  and *saddle quantity*  $\sigma = \lambda_s + \lambda_u$ . It can be shown [35] that for  $\sigma < 0$ , or  $\nu > 1$ , at the side of the saddle-loop bifurcation where one has a detached cycle, this cycle is stable, while for  $\sigma > 0$  ( $\nu < 1$ ), the cycle is unstable. Analogously, one can study the period of the cycle close to this bifurcation, and to leading order it is given by [27],

$$T \propto -\frac{1}{\lambda_u} \ln |\theta - \theta_{SL}|. \quad (2)$$

This expression is accurate for  $\theta$  close enough to  $\theta_{SL}$ . Interestingly, the transient times spent by a trajectory in the ghost region after the cycle has ceased to exist, close enough to the bifurcation point, also show this scaling.

From a numerical viewpoint, we will characterize the occurrence of a saddle-loop bifurcation in the system by studying the scaling of the period of the oscillations. The bifurcation point will be characterized by the fact that approaching from the oscillatory side the period diverges to infinity, and also because past this bifurcation point the LS disappears and the system relaxes to the homogeneous solution as shown in Fig. 5 for  $I_s = 0.9$ . For this value of  $I_s$  the saddle-loop takes place at  $\theta_{SL} = 1.30478592$ . In the figure the time evolution of the maximum of the LS is plotted for two values of the detuning differing in  $10^{-7}$ , one just above and the other just below  $\theta_{SL}$ . Figure 6 contains a logarithmic-linear plot of the period versus a control parameter, that exhibits, as expected, a linear slope. Furthermore, one can confront the value of the slope obtained from the simu-

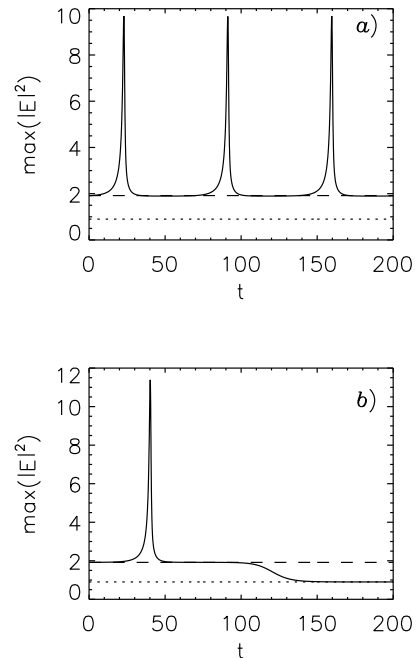


FIG. 5: Maximum intensity of the LS as function of time for  $I_s = 0.9$ . a) Oscillatory trajectory for  $\theta = 1.3047859$  (just below  $\theta_{SL}$ ). b) Excitable trajectory starting from an initial condition very close but above the saddle point in the phase space ( $\theta = 1.3047860$ , just above  $\theta_{SL}$ )

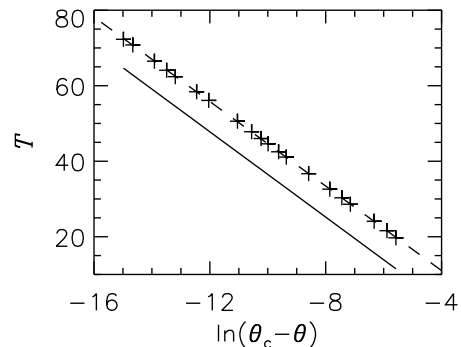


FIG. 6: Scaling of the period in the saddle-loop bifurcation. Crosses correspond to numerical simulations while the solid line, arbitrarily positioned, has a slope  $1/\lambda_u$  with  $\lambda_u = 0.177$  obtained from the stability analysis of the unstable LS.

lations with its theoretical prediction, Eq. (2), namely  $1/\lambda_u$ . The full spectrum of the middle branch soliton for  $\theta = \theta_{SL}$  (calculated as described in the Appendix) is shown in Fig. 4. The agreement between the simulations and theoretical slopes is within 1%.

A comment is in place here regarding the spectrum shown in Fig. 4. The spectrum is formed by a stable continuous (although numerically discretized) and a dis-

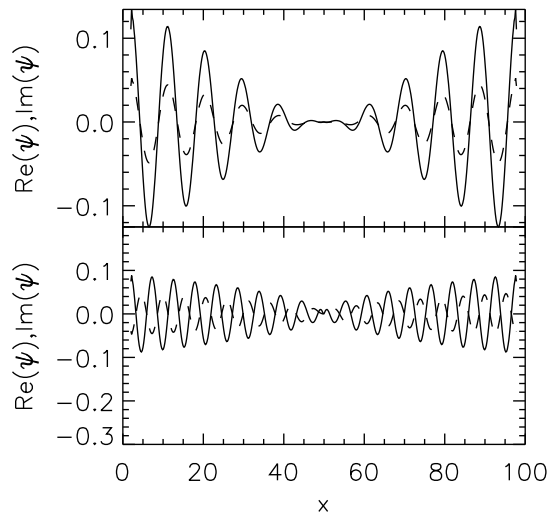


FIG. 7: Stable extended modes from the continuous band. The top (bottom) panel shows the transverse cut of the mode associated to the eigenvalue  $\lambda = -0.1$  ( $\lambda = -1 + i0.24$ ) of Figure 4. The solid (dashed) line indicates the real (imaginary) parts of the eigenmode.

crete spectrum with a positive ( $\lambda_u = 0.177$ ) and a negative ( $\lambda_s = -2.177$ ) eigenvalue. Having this spectrum in mind is perhaps surprising that one can describe the bifurcation route very well qualitatively, and to some extent quantitatively (cf. the observed scaling law, Fig. 6), resorting to a planar dynamical system when many modes could be, in principle, involved. The first mode of the planar theory univocally corresponds to the positive (unstable) eigenvalue,  $\lambda_u = 0.177$ , while, in first approximation, the second mode should correspond to the second, closest to zero, eigenvalue. This eigenvalue belongs however to a continuum band and the arbitrarily close eigenvalues of its band could play a role in the dynamics, modifying the planar theory. Moreover, considering this mode  $\lambda \sim -0.10$  the saddle-index  $\nu = -\lambda/\lambda_u < 1$  indicating that the cycle emerging from the saddle-loop should be unstable, although we observe otherwise. The analysis of the modes of the unstable LS and dimensionality of the phase space is addressed in detail in the next section.

## V. MODE ANALYSIS

In this section we analyze the dynamics in terms of the modes obtained in performing the stability analysis of the middle branch LS in a parameter region close to the saddle-loop bifurcation, as described in Appendix A. By plotting the spatial profile of the modes one obtains a clue to identify the relevant modes for the dynamics. It turns out that most of the modes of the stable spectrum are delocalized. Figure 7 contains a representation of two such delocalized modes. The bands of extended modes

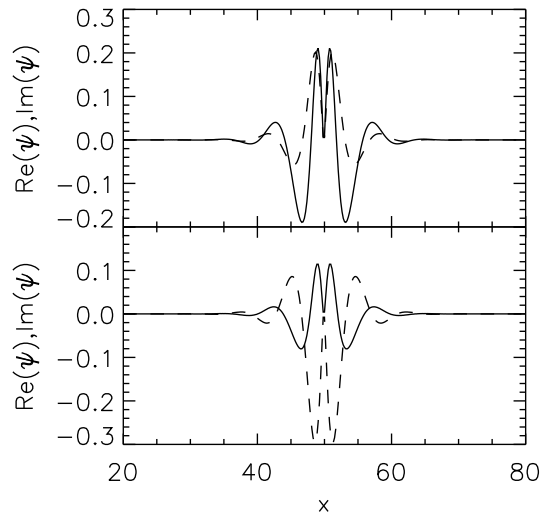


FIG. 8: Transverse cut of the unstable (top) and the most stable (bottom) modes of the unstable LS. These modes are associated to the eigenvalues  $\lambda_u = 0.177$  and  $\lambda_s = -2.177$  of Fig. 4 respectively. The solid (dashed) line indicates the real (imaginary) parts of the eigenmode.

correspond to modes of the homogeneous background, and are, except for a radial dependence coming from the fact that we are using radial instead of Cartesian coordinates, basically Fourier modes. The main difference between these modes is the wavenumber of their oscillations (see Fig. 7). There are however two exceptions: two localized modes which are the one corresponding to the unstable direction and the most stable mode, namely that with eigenvalue  $\lambda_s = -2.177$ . The spatial profile of these two modes is shown in Figure 8. Since the dynamics of the LS remains localized in the space, this is an indication that only these two localized modes take part in the dynamics. To check this hypothesis we have projected the two trajectories shown in Fig. 5 for parameters close to the saddle-loop bifurcation onto all the eigenmodes of the unstable LS and observed that only the two localized modes have a significant amplitude.

From the knowledge of the spectrum and the relevant eigenmodes, we can now explain the stability of the orbits emerging out of the bifurcation, namely through the saddle index introduced above. Computing this index for the two modes that participate in the saddle-loop bifurcation one obtains  $\nu = 2.177/0.177 > 1$ , what fits perfectly with the fact that the cycle that detaches at one side of the bifurcation point is stable. Thus, one may understand that all the dynamical instability scenario of the LS can be analyzed qualitatively in a planar dynamical system.

A better understanding of the dynamical route, and a justification of the role of the two participating localized modes, stable and unstable, can be obtained through a closer scrutiny of the *linear* region, namely the region close to the saddle point (or alternatively, the region defined by the singular map, or close to it). Figure 5a

contains a time trace of one such trajectory in the region in which the limit cycle is stable, but close to the saddle-loop bifurcation. Following Appendix A we project the deviation of the trajectory from the unstable LS (saddle point) onto the most stable and the unstable eigenvectors of the adjoint Jacobian matrix of the unstable LS. These projections are the amplitudes of the unstable ( $\beta_1$ ) and the most stable ( $\beta_2$ ) modes of the unstable LS (modes whose profile is shown in Fig. 8). The trajectory enters the linear region through the stable mode and leaves the region through the unstable one. This behavior is clear in the insets of Figure 9. Next, we reconstruct the qualitative sketch of the bifurcation shown in Fig. 2 of [16] from the knowledge of the projections onto the modes, i.e. we represent the trajectories before and after the saddle-loop bifurcation in mode space. Thus, Figure 9 contains a quantitative, reconstructed, 2-dimensional phase space from the two localized modes involved in the transition for a set of parameter values in the a) oscillatory and b) excitable side of the transition. Close to the saddle, the linear dynamics takes place on a plane, but away from this point the nonlinear dynamics bends the trajectory out of the plane into the higher dimensional space, hence, the apparent crossing of the trajectory in Fig. 9.

This is the final numerical confirmation that the infinite-dimensional dynamical system on which LS live can be reduced to an excellent degree of precision to a 2-dimensional dynamical system, and that the picture is fully consistent with a saddle-loop bifurcation.

## VI. EXCITABLE BEHAVIOR

As in our case the saddle-loop bifurcation involves a fixed point (the homogeneous solution), on one side of the bifurcation, and an oscillation, on the other, the system is a candidate to exhibit excitability [18]. It must be stressed that excitable behavior is not guaranteed *per se* after a saddle-loop bifurcation, and, in particular one needs a fixed point attractor that is close enough to the saddle point that destroys the oscillation. The excitability threshold in this type of system is the stable manifold of the saddle point, what implies that the observed behavior is formally Class I Excitability [18], i.e., the excitability is characterized by response times that can be infinite (if a perturbation hits exactly the stable manifold of the fixed point), or, conversely, frequencies starting from zero. In our system, the excitable threshold reduces by increasing  $I_s$  (Fig. 2), since the middle branch LS (the saddle point) gets progressively closer to the homogeneous solution (fixed point).

This excitability scenario was shown in Ref. [16], and in parameter space it is found in the region above the dashed line corresponding to the saddle-loop bifurcation shown in Fig. 1. Fig. 10 shows the resulting trajectories after applying a localized perturbation in the direction of the unstable LS with three different amplitudes: one below the excitability threshold (a), and two above: one

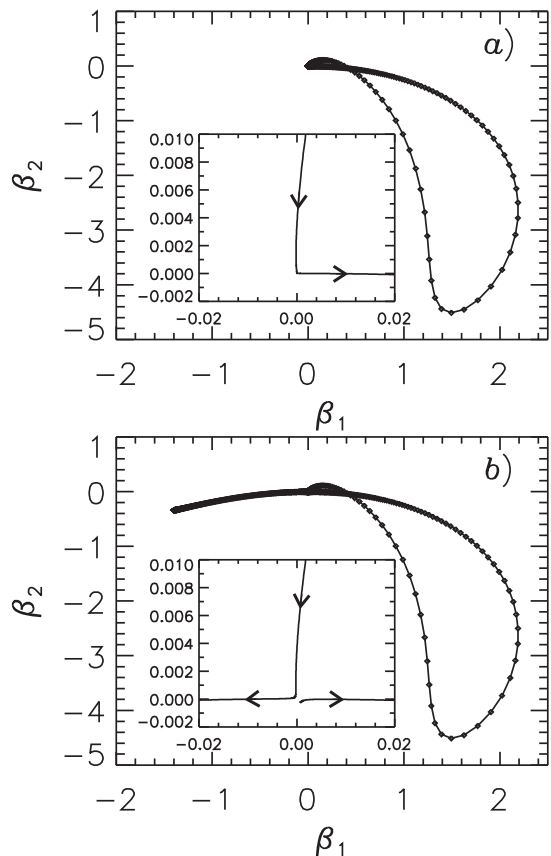


FIG. 9: Reconstructed phase space by finding the amplitude of the deviation of the trajectory from the unstable LS in the unstable ( $\beta_1$ ) and the most stable ( $\beta_2$ ) modes of the unstable LS. Panel a) corresponds to an oscillatory trajectory while panel b) to an excitable one. The symbols are equispaced in time along the trajectory, so sparse symbols indicate fast dynamics while dense symbols indicate slow dynamics. The saddle point is at (0,0). The inset is a close up of the linear region around the saddle.

very close to threshold (b) and the other well above (c). For the below-threshold perturbation the system decays exponentially to the homogeneous solution, while for the above-threshold perturbations a long excursion in phase space is performed before returning to the stable fixed point. The refractory period for the perturbation just above the excitability threshold is appreciably longer due to the effect of the saddle. The spatio-temporal dynamics of the excitable localized structure is shown in Fig. 11. After an initial localized excitation is applied, the peak grows to a large value until the losses stop it. Then it decays exponentially until it disappears. A remnant wave is emitted out of the center dissipating the remaining energy.

At this point it is worth noting that neglecting the spatial dependence Eq. (1) does not present any kind of excitability. The excitable behavior is an emergent property of the spatial dependence and it is strictly related to the dynamics of the 2D LS. Without spatial dependence,

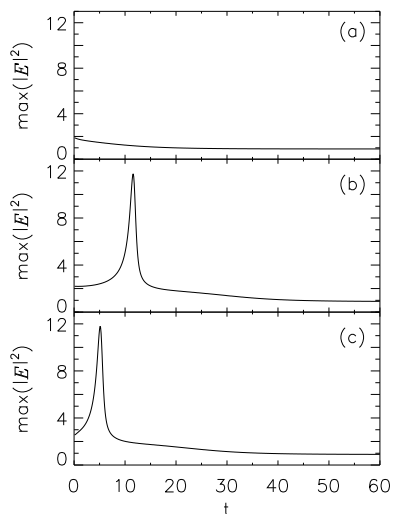


FIG. 10: Time evolution of the maximum intensity starting from the homogeneous solution ( $I_s = 0.9$ ) plus a localized perturbation of the form of the unstable LS multiplied by a factor 0.8 (a), 1.01 (b) and 1.2 (c).

excitability as a result of a saddle-loop bifurcation has been observed in different systems [17, 18, 28].

Finally, it is interesting to remark that the excitable region in parameter space is quite large (cf. Fig. 1) and, therefore, potentially easy to observe experimentally. While this excitable behavior belongs to Class I (the period diverges to infinity when a perturbation hits the saddle), due to the logarithmic scaling law for the period (2), the parameter range over which the period increases dramatically is extremely narrow (cf. Fig. 3(a) in Ref. [16]). Therefore, from an operational point of view, systems exhibiting this scenario might not be classified as Class I excitable, as the large period responses may be easily missed [29].

## VII. TAKENS-BOGDANOV POINT

The saddle-loop (or homoclinic) bifurcation is, in some sense, not *generic*. Namely, that a tangency between a limit cycle and a saddle point occurs exactly such that it happens simultaneously at both the sides of the stable and unstable manifolds is, in principle, not to be expected generically. In fact, also due to the fact that global bifurcations are not always easy to detect, showing that a dynamical system exhibits a certain type of codimension-2 point is the most convincing argument for the existence of such bifurcations.

An scenario in which the unfolding of a codimension-2 point yields a saddle-loop (or homoclinic) bifurcation is a Takens-Bogdanov (TB) point [30, 31]. Namely, a double-zero bifurcation point in which a saddle-node bifurcation line and the zero-frequency limit of a Hopf bifurcation line (thus, no longer a Hopf line in the crossing point) meet in a two-parameter plane. The partic-

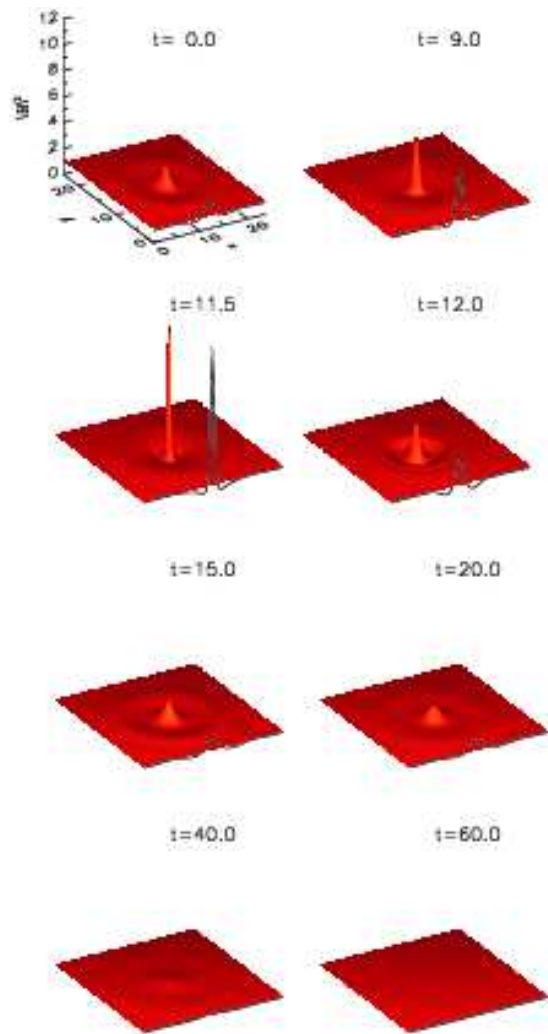


FIG. 11: (Color online) 3D plots showing the transverse intensity profile at different times for the trajectory shown in Fig. 10(b). The solid lines show a cut of the structure through the center.

ular feature that, at the TB point, the Hopf line has zero frequency allows this codimension-2 bifurcation to occur in a two-dimensional phase space. This bifurcation has to be distinguished from the occurrence of a crossing between a saddle-node and a Hopf lines at non-zero frequency, known as Gavrilov-Guckenheimer (saddle node-Hopf point), that requires a three-dimensional phase space to take place. One can prove that from the unfolding of a TB point a saddle-loop line, apart from the saddle-node and Hopf lines, emerges [30, 31] from the TB point.

This can be checked in Fig. 1, in which a two-parameter bifurcation plot is presented as a function of the two parameters of the system:  $I_s$  and  $\theta$ . The problem here is that the saddle-node and Hopf lines tend to meet only asymptotically, namely when  $\theta \rightarrow \infty$ . In Ref. [16] we checked already that the distance between the saddle-node and the Hopf lines decreases as one increases  $\theta$  (the

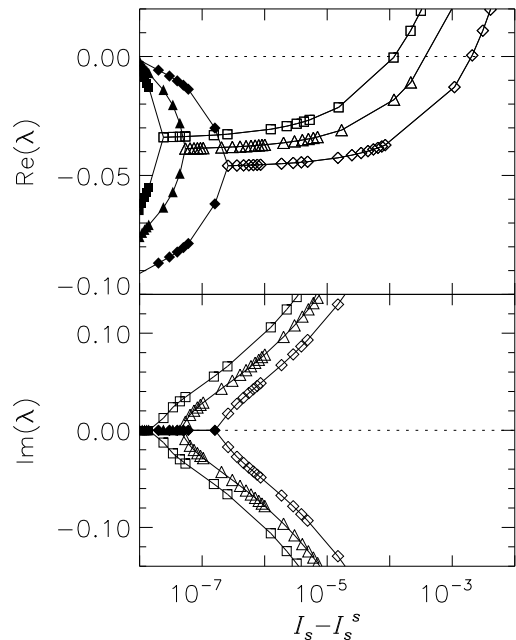


FIG. 12: Real part (upper panel) and imaginary part (lower panel) of the eigenvalues of the upper branch LS for three vertical cuts in Fig. 1 corresponding to three different values  $\theta$ : squares, 1.7; triangles, 1.5; rhombs, 1.4 versus the difference between  $I_s$  and its value at the saddle-node bifurcation,  $I_s - I_s^s(\theta)$ .

same happens with the saddle-loop line). By calculating the eigenvalues, it can be seen that, indeed the frequency (viz. their imaginary part) goes to zero as one approaches the TB point. Fig. 12 displays the two eigenvalues with largest real part of the upper branch LS for parameter values corresponding to three vertical cuts of Fig. 1. Open symbols correspond to eigenvalues with a non-zero imaginary part while filled symbols are associated to real eigenvalues. Where the open symbols cross zero in the upper panel of Fig. 12 signals the Hopf bifurcation while where the filled symbols cross zero signals the saddle-node bifurcation. The origin for the three plots is taken at the saddle-node bifurcation. At some point along the branch of the two complex conjugate eigenvalues associated to the Hopf bifurcation the imaginary part vanishes leading to two branches of real eigenvalues, the largest of which is precisely the responsible of the saddle-node bifurcation. As detuning increases the Hopf and saddle-node bifurcation points gets closer and closer but the structure of eigenvalues remains unchanged so that when the Hopf and saddle-node bifurcation will finally meet the Hopf bifurcation will have zero frequency, signaling a TB point.

The TB point takes place asymptotically in the limit of large detuning  $\theta$  and small pump  $E_0$ . In this limit Eq. (1) becomes the conservative NLSE [10]. The Hopf instability in this limit was studied in [24], where evidence of

the double-zero bifurcation point was given, however the unfolding leading to the scenario presented here was not analyzed.

## VIII. CONCLUDING REMARKS

In this work a detailed study of the instabilities of LS solutions in homogeneously pumped nonlinear Kerr cavities and the associated excitability route first reported in Ref. [16] is carried out. In that study, it was shown that the instability that leads to the destruction of oscillatory LS found in this system can be characterized by a saddle-loop (homoclinic) bifurcation, in which, in phase space, the oscillation (a limit cycle) becomes the homoclinic orbit of a saddle point. This scheme is able to explain accurately quantitative aspects of the transition, like scaling law for the divergence of the period of the oscillation at the bifurcation point.

After a close scrutiny there is at least an aspect that may sound puzzling in this picture: the system under study is described by a 2-D nonlinear Partial Differential Equation, with an infinite-dimensional phase space. Instead, the reported saddle-loop bifurcation minimally needs a 2-D dimensional system with a limit cycle and a saddle point, what is coherent with the fact that the bifurcation *is born* at a Takens-Bogdanov codimension-2 point. One can devise a kind of slaving principle, in which the slowest modes (with the closest eigenvalues to zero) dominate the slow dynamics. However, the two leading eigenvalues of the saddle point close to bifurcation do not explain the scenario (give the wrong stability for the limit cycle). For all this, we have engaged in showing the reason why such a 2-dimensional reduction is successful in explaining the dynamics, and, in particular, what happens with the stability of the emerging limit cycle.

The main result of this paper is that it is possible to recover quantitatively, from the full system, the qualitative 2-dimensional sketch of the saddle-loop bifurcation, in which two modes participate: the single unstable mode, and a kind of conjugate stable mode (buried in the sea of stable modes), with the property that both modes are the only two localized modes of the system.

Apart from this kind of fundamental result, the main interest of the present work is to prove excitability in an extended system as an emerging property, *i.e.*, not present locally in the spatio-temporal system, but emerging through one of its solutions. Excitability is possible in classes of systems in which an oscillation is destroyed at a bifurcation yielding, at the other side, a fixed point solution. In the present scenario, mediated by a saddle-loop bifurcation, excitability is not generic, and requires the availability of a close enough fixed point solution: the homogeneous solution, in the present case.

### Acknowledgments

We thank D. Pazó for useful discussions. We acknowledge financial support from MEC (Spain) and FEDER: Grants FIS2004-00953 (CONOCE2), FIS2004-05073-C04-03, FIS2006-09966, and TEC2006-10009 (PhoDeCC). AJ acknowledges financial support from MEC.

### Appendix A

In this appendix we describe in some detail the numerical methods used throughout this paper.

For numerical simulations, we integrate Eq. (1) using a pseudo-spectral method where the linear terms in Fourier space are integrated exactly while the nonlinear ones are integrated using a second-order in time approximation [32]. Periodic boundary conditions are used, since they are convenient for the pseudospectral code. The system size is large enough to ensure that the electric field reaches the homogeneous steady state well before the boundaries. A square lattice of size  $512 \times 512$  points was used. The space discretization was taken  $dx = 0.1875$  while the time step was  $dt = 10^{-3}$

To study the stability of the stationary LS solutions of Eq. (1), we set  $E = E_s(1 + A)$ , so that  $A(x, y)$  describes the solution without the homogeneous background,

$$\frac{\partial A}{\partial t} = -(1 + i\theta)A + i\nabla^2 A + iI_s(2A + A^* + A^2 + 2|A|^2 + |A|^2 A), \quad (3)$$

where Eq. (3) is obtained directly from Eq. (1), without any approximation. To obtain the stationary solutions one may numerically solve the rhs of Eq. (3) equated to zero. However, since we have 2 spatial dimensions and the self-focusing dynamics involve very large wavenumbers with very fast dynamics, this is a difficult and time consuming task. Instead, we can take advantage of the fact that the LS structures are rotationally symmetric with respect to their center, so that they can be described in terms of the 1D radial equation for  $A(r)$

$$\frac{\partial A}{\partial t} = -(1 + i\theta)A + i\left(\frac{\partial^2}{\partial^2 r} + \frac{1}{r}\frac{\partial}{\partial r}\right)A + iI_s(2A + A^* + A^2 + 2|A|^2 + |A|^2 A). \quad (4)$$

Steady state LS solutions for this system, both stable and unstable, are found by equating to zero the lhs of Eq. (4). The boundary conditions for this problem are such that the derivatives are zero at the boundaries, i.e.,  $\partial A/\partial r(r=0) = \partial A/\partial r(r=L) = 0$ , where the system size  $L$  is large enough to ensure that the electric field approaches smoothly the homogeneous solution ( $A(r) \rightarrow 0$ ) before reaching the boundary.

The stability of steady state LS against radial and azimuthal perturbations is obtained, cf. Ref. [33], by

linearizing Eq. (3) around the corresponding, numerically obtained, stationary solution  $A_{LS}$ . This yields a linearized equation for the time evolution of the perturbations  $\delta A(r, \phi, t) = A(r, \phi, t) - A_{LS}(r)$ . The solutions of the linear problem can be written as

$$\delta A = [R_+(r)e^{im\phi} + R_-(r)e^{-im\phi}] \exp(\lambda t), \quad (5)$$

where  $m$  is the wavenumber of the azimuthal perturbation. This yields the eigenvalue problem

$$\mathbf{U}\Psi = \lambda\Psi \quad (6)$$

where  $\Psi = (R_+, R_-)^T$  and  $\mathbf{U} = \begin{pmatrix} U_+ & U_- \\ U_-^\dagger & U_+^\dagger \end{pmatrix}$ , with

$$\begin{aligned} U_+ &= -(1 + i\theta) + i\left(\frac{\partial^2}{\partial^2 r} + \frac{1}{r}\frac{\partial}{\partial r} - \frac{m^2}{r^2}\right) \\ &\quad + i2I_s(1 + A_{LS} + A_{LS}^* + |A_{LS}|^2) \\ U_- &= iI_s(1 + 2A_{LS} + A_{LS}^2), \end{aligned} \quad (7)$$

is the Jacobian. For purely radial perturbations ( $m=0$ )  $R_- = R_+$ . The matrix  $\mathbf{U}$  is time-independent as it is evaluated at the stationary LS (stable or unstable) under study.

The problem reduces, thus, to finding the eigenvalues,  $\lambda$ , and eigenvectors,  $\Psi$ , where it is important to mention that  $\mathbf{U}$  is a complex matrix and, thus, the eigenvectors are complex quantities in general. Due to the symmetry of  $\mathbf{U}$  the eigenvalues are either real or pairs of complex conjugates. This last property stems from the fact that, considering the real and imaginary parts of  $A_{LS}$ ,  $\mathbf{U}$  can be rewritten as a real matrix. We note also that, due to the discretization of the space,  $\Psi$  becomes a vector whose dimension is  $2N$ . The set of eigenvectors  $\Psi_i$  ( $i=1, 2N$ ) form a basis, and their amplitudes define a natural phase space where studying the dynamics of LS.

However,  $\mathbf{U}$  is not a self-adjoint operator so, the set of eigenmodes does not form an orthogonal basis. To find the components of a field profile on a mode  $\Psi_i$  one has to project it onto the corresponding eigenmode  $\Phi_i$  of the adjoint Jacobian matrix  $\mathbf{U}^\dagger$ . In Section V we are interested in the deviation of the field profile from the unstable LS (saddle point)  $\delta\mathbf{A} = (\delta A, \delta A^*)^T$ . In particular we calculate the components of this deviation on the unstable and the most stable eigenmodes of the Jacobian matrix of the unstable LS. These amplitudes are given by  $\beta_i = \int \Phi_i^{\dagger*} \cdot \delta\mathbf{A} dr$  ( $i=1, 2$ ), where  $\Phi_1$  is the unstable and  $\Phi_2$  the most stable eigenmodes of the adjoint Jacobian matrix.

We should note that in the work reported here the LS are always inside the region in which they are stable versus azimuthal perturbations [12], so all the instabilities described in the text are obtained for  $m=0$ . As final comment, the stability problem of stationary LS, that in principle live in an infinite-dimensional phase space, is reduced numerically to a stability problem in a finite-dimensional, albeit large, phase space.

- 
- [1] O. Thual and S. Fauve, *J. Phys. (France)* **49**, 1829 (1988).
- [2] J. E. Pearson, *Science* **261**, 189 (1993).
- [3] K. J. Lee and H. L. Swinney, *Science* **261**, 192 (1993).
- [4] I. Müller, E. Ammelt, and H. G. Purwins, *Phys. Rev. Lett.* **82**, 3428 (1999).
- [5] M. Tlidi, P. Mandel, and R. Lefever, *Phys. Rev. Lett.* **73**, 640 (1994).
- [6] S. Barland *et al.*, *Nature (London)* **419**, 699 (2002).
- [7] W. J. Firth and C. O. Weiss, *Opt. Photon. News* **13**, 55 (2002).
- [8] P. Couillet, C. Riera, and C. Tresser, *Chaos* **14**, 193 (2004).
- [9] C. Sulem and P. L. Sulem, *The Nonlinear Schrödinger Equation* (Springer, New York, 1999).
- [10] W. J. Firth and A. Lord, *Journal of Modern Optics* **43**, 1071 (1996).
- [11] W. J. Firth, A. Lord, and A. J. Scroggie, *Physica Scripta* **67**, 12 (1996).
- [12] W. J. Firth, G. K. Harkness, A. Lord, J. M. McSloy, D. Gomila, and P. Colet, *J. Opt. Soc. Am. B* **19**, 747 (2002).
- [13] P. B. Umbanhowar, F. Melo, and H. L. Swinney, *Nature (London)* **382**, 793 (1996).
- [14] S. Longhi, G. Steinmayer, and W. S. Wong, *J. Opt. Soc. Am. B* **14**, 2167 (1997).
- [15] V. K. Vanag and I. R. Epstein, *Phys. Rev. Lett.* **92**, 128301 (2004).
- [16] D. Gomila, M. A. Matías, and P. Colet, *Phys. Rev. Lett.* **94**, 063905 (2005).
- [17] J. Rinzel and G. B. Ermentrout, in *Methods in Neuronal Modeling*, edited by C. Koch and I. Segev (MIT Press, Cambridge, MA, 1989).
- [18] E. M. Izhikevich, *Int. J. Bif. Chaos* **10**, 1171 (2000).
- [19] L. A. Lugiato and R. Lefever, *Phys. Rev. Lett.* **58**, 2209 (1987).
- [20] J. J. Rasmussen and K. Rypdal, *Phys. Scr.* **33**, 481 (1986).
- [21] A. J. Scroggie, *Chaos, Solitons, and Fractals* **4**, 1323 (1994).
- [22] P. D. Woods and A. R. Champneys, *Physica D* **129**, 147 (1999).
- [23] P. Couillet, C. Riera, and C. Tresser, *Phys. Rev. Lett.* **84**, 3069 (2000).
- [24] D. V. Skryabin, *J. Opt. Soc. Am. B* **19**, 529 (2002).
- [25] P. Glendinning, *Stability, instability, and chaos* (Cambridge U.P., Cambridge, UK, 1994).
- [26] S. Wiggins, *Global bifurcations and chaos: analytical methods* (Springer-Verlag, New York, 1988).
- [27] P. Gaspard, *J. Phys. Chem.* **94**, 1 (1990).
- [28] F. Plaza, M. G. Velarde, F. T. Arecchi, S. Boccaletti, M. Ciofini and R. Meucci, *Europhys. Lett.* **38**, 85 (1997).
- [29] E. M. Izhikevich, *Dynamical Systems in Neuroscience* (MIT Press, Cambridge (MA), 2006).
- [30] J. Guckenheimer and P. Holmes, *Nonlinear Oscillations, Dynamical Systems, and Bifurcations of Vector Fields* (Springer, New York, 1983).
- [31] Y. A. Kuznetsov, *Elements of Applied Bifurcation Theory, 2nd ed.* (Springer Verlag, New York, 1998).
- [32] R. Montagne, E. Hernández-García, A. Amengual, and M. San Miguel, *Phys. Rev. E* **56**, 151 (1997).
- [33] J. M. McSloy, W. J. Firth, G. K. Harkness, and G. L. Oppo, *Phys. Rev. E* **66**, 046606 (2002).
- [34] The Poincaré map can be constructed through two cross sections, i.e., two planes that are transversal to the limit cycle, and that are placed slightly before and after the closest approach of the cycle to the saddle point. From these two planes one can construct two maps: the so-called local (or linear or singular) map,  $T_0$ , that takes the flow from the plane before the saddle point to the plane after the saddle point, and it is dominated by the saddle point, and the global (or nonlinear) map,  $T_1$ , that takes the flow all the way from the plane past the saddle point through all the limit cycle back to the plane before the saddle point. The complete Poincaré map is the composition of these two maps. It has to be remarked that the  $T_0$  map is unbounded, as the return time is infinity at the onset of the global bifurcation.
- [35] For the details refer, e.g., to Sec. 12.3 of Ref. [25]